Nuclear Inst, and Methods in Physics Research B 431 (2018) 31–37

Contents lists available at ScienceDirect

Nuclear Inst. and Methods in Physics Research B

journal homepage: www.elsevier.com/locate/nimb

A comparison of the analysis of non-centrosymmetric materials based on ion and electron beams

Henrique Trombini[a,*], Pedro Luis Grande[a], Agenor Hentz[a], Maarten Vos[b], Aimo Winkelmann[c]

[a] Ion Implantation Laboratory, Institute of Physics, Federal University of Rio Grande do Sul, Av. Bento Gonçalves 9500, CP 15051, CEP 91501-970 Porto Alegre, RS, Brazil

[b] Electronics Materials Engineering, Research School of Physics and Engineering, The Australian National University, Canberra 0200, Australia

[c] Bruker Nano GmbH, Am Studio 2D, Berlin 12489, Germany

ARTICLE INFO

Keywords:
Medium energy ion scattering
Non-centrosymmetric materials
GaP
Cartography

ABSTRACT

Techniques like electron backscattered diffraction (EBSD) and angle-resolved electron Rutherford backscattering (ERBS) are sensitive to the lack of inversion symmetry in crystals and hence can determine the absolute crystal orientation. In this paper we demonstrate for the case of GaP that medium energy ion scattering (MEIS) can also be used to obtain the absolute crystal orientation. A comparison between the 2D-backscattering intensities as a function of the detection directions for electrons (as is measured in EBSD or ERBS) and protons (as is measured in MEIS) is made and discussed in terms of diffraction and classical subchanneling respectively.

1. Introduction

In contrast to centrosymmetric semiconductors with the diamond structure (point group $m\bar{3}m$), the $\langle 001 \rangle$ axes cease to be proper 4-fold rotation axes for binary semiconductors like GaAs and GaP crystallizing in the cubic zincblende structure (point group $\bar{4}3m$). In the zincblende structure, a rotation over 90° around $\langle 001 \rangle$ is equivalent to an inversion operation, which can effectively interchange the relative position of the cations and anions.

An important consequence of the symmetry reduction in the zincblende as compared to the diamond structure is relevant, for example, when films of III-V compounds are grown on a Si(001) surface [1]. In this case, domains of two inequivalent crystal orientations related by an inversion operation can be formed in the overlayer, and defects will be found at the anti-phase domain boundaries. It is thus important to be able to characterize the absolute orientation of crystals experimentally, which requires a characterization method that is sensitive to the absence of a center of symmetry in the crystal structure.

For imaging applications in the scanning electron microscope (SEM), it was shown recently that electron backscatter diffraction (EBSD) can be used to map the distribution of anti-phase domains in thin GaP films [2]. Dynamical electron diffraction effects in the Kikuchi diffraction patterns which are observed in an EBSD measurement can provide sensitivity to non-centrosymmetric effects of the crystal structure. By correlating experimentally observed two-dimensional Kikuchi diffraction patterns with simulations using the dynamical theory of electron diffraction, the local absolute crystal orientation can be assigned to the measured sample region.

Moreover, in Electron Rutherford Backscattering (ERBS) experiments it was shown that, if one separates the contribution of the anion and cation based on their different recoils losses, the effect of the orientation has the opposite sign for scattering from the cation and anion [3]. As the strength of both signals depend on their atomic number Z, a small fraction of this asymmetry survives if one takes the sum of both intensities, as is done in conventional EBSD. This small difference is enough, however, to determine completely the overlayer orientation.

Ion channeling is a real-space technique that can probe the crystal structure. Here recoil effects are much larger (due to the smaller mismatch of the mass of projectile and target atom) and separation of the heavy and light atoms is more routinely obtained. Can ion-beam techniques be an alternative to EBSD for the determination of the overlayer orientation and what is the nature of the difference under these conditions? Here we explore this question using medium energy ion scattering (MEIS) with an electrostatic analyzer. Then it is possible to obtain two-dimensional intensity distributions, just as in EBSD, but only for the contribution of the heavier element. To be specific we studied a bulk GaP crystal using 100 keV protons as a projectile and focus on the deviations of the observed intensity, when the crystal is rotated by 90° along the [100] axis, i.e. if it is possible to determine the complete crystal orientation.

Asymmetries measured by ion channeling have been reported before for non-centrosymmetric crystals [4–6] for angular scans. Here we

* Corresponding author.
E-mail address: henrique.trombini@ufrgs.br (H. Trombini).

https://doi.org/10.1016/j.nimb.2018.06.026
Received 5 April 2018; Received in revised form 8 June 2018; Accepted 26 June 2018

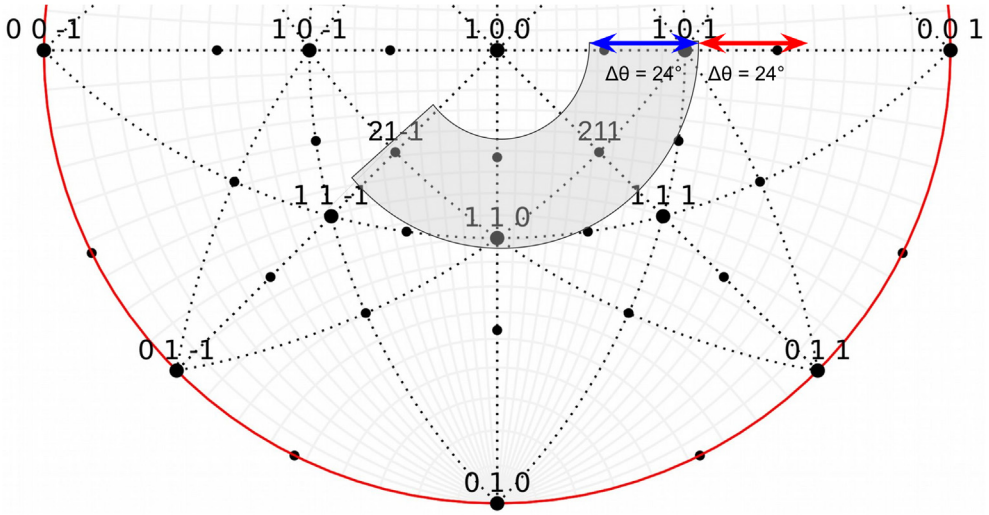

Fig. 1. Stereographic projection of the GaP crystal on the [100] direction. The shaded area corresponds to the region where the experimental cartography was performed. The red and blue arrows show the polar angle regions for a normal incidence beam and for a 25° tilt in the sample, respectively [9]. (For interpretation of the references to colour in this figure legend, the reader is referred to the web version of this article.)

measure complete two-dimensional intensity distributions over a range of (θ, ϕ) angles.

2. Experimental procedure

The MEIS measurements were performed at the Ion Implantation Laboratory of the Federal University of Rio Grande do Sul. A 500 keV electrostatic accelerator provided an incident beam of H^+ with an energy of 99 keV. The GaP crystal was mounted on a 3-axis goniometer that allowed us to perform measurements with the outgoing trajectories along different polar and azimuthal angles. The pressure in the analysis chamber was about 10^{-7} mbar. Typical beam currents were less than 15 nA. The backscattered H^+ ions were analyzed with a Toroidal Electrostatic Analyzer (TEA). At the exit plane of the TEA a pair of micro-channel plates coupled to a position-sensitive detector was used to measure the scattering energy and angle for the detected ions [7,8]. The analyzer is mounted at 120° with respect to the incident beam. The TEA angular aperture is 24° and each angle bin corresponds to 0.08°. These configuration allows the analysis in a polar range from $\theta = 48°$ to 72°, as shown by red arrows in the Fig. 1. In order to perform the analysis in a different polar range we rotated the sample towards the detector by 25°. Then a polar range between 23 and 47° is measured, as shown by the blue arrows in Fig. 1. The overall energy resolution of the system is 450 eV for 99 keV H^+ ions.

Typical maps of ion scattering intensities as a function of the detected energies and scattering angles (the so-called 2D MEIS spectra) for 99 keV H^+ ions impinging on GaP crystal are shown in Fig. 2.

Blocking lines (reduced intensity at certain scattering angles) are evident in the top panel. Corresponding PowerMeis [10] simulations for an amorphous GaP are shown on the bottom panel. The region 1 corresponds to the surface peak of Ga and the region 2 to the surface peak of *P* superimposed to the Ga signal. The contributions from H^+ backscattering from Ga and from the combination of Ga and P are easily distinguished and were used to select the energy window for the cartography. In the energy range indicated as region 1 the H^+ was backscattered from Ga near the surface.

The difference between the experiment (top panel) and simulation in region 1 is due to channeling and blocking effects. In this experiment the incoming beam was along the surface normal, i.e. the ⟨100⟩ directions and the scattering yield away from the surface was reduced by the channeling effect (at all scattering angles). In addition, blocking causes the reduction of the ion scattering intensity for certain scattering angles (evident as vertical lines with reduced intensity). Since the simulation is for an amorphous GaP sample the ion scattering intensity is only affected by a slow decrease in the scattering cross section with increasing polar angle. The onset of the P contribution to the spectrum occurs several keV below the onset of the Ga contribution. The change of the onset with the scattering angle is described by the kinematic factors of Ga and P. If one adds add up measurements taken at different azimuthal angles (here varied from 0° to 90°, with a step of 5°), then the blocking effect are averaged out, as shown in Fig. 2 (middle panel). However, this procedure does not eliminate channeling effects as evident by the reduced intensity near 90 keV, below the Ga surface peak. The comparison between this experimental result and the simulation shows more clearly the contribution from Ga and Ga plus P signals. Also the cross-section dependence on the scattering angle is more clearly revealed in the simulation.

In order to obtain a map of the blocking directions of the GaP crystal, and thus to determine its stereographic projection, we followed the procedure described in detail in Refs. [11,12]. In short, the 2D-MEIS spectrum (as shown in Fig. 2 top panel, but now with the crystal rotated so the incoming beam is 25° away from the surface normal and generally not along a channeling direction) is measured. The intensity $I(\theta)$ in a selected energy range of $91.5 < E < 93.0$ is recorded. Then the crystal is rotated along the surface normal, and in this way the azimuthal (ϕ) angle is scanned over 142° with increments $\Delta\phi$ of 0.5°. The measured angular range is showed as a shaded area in the Fig. 1. The selected energy range corresponds to a backscattering depth of $\simeq 6 \pm 1.5$ nm for a scattering angle of 120°. In this energy window (region 1) only Ga contributes, as shown in Fig. 2. Changing the azimuthal angle also changes the direction of the incoming beam. For each azimuthal angle, blocking lines were observed on the 2D-MEIS spectrum at specific polar angles. For some azimuthal angle the incoming beam coincides with a planar direction and there was a clear channeling effect observable, causing reduced intensity for all polar values. By combining the $I(\theta)$ obtained at different ϕ angles, we obtain the $I(\theta, \phi)$ distribution that represents the cartography of the crystal.

3. Theoretical procedure

The MEIS cartography was compared with results of Monte-Carlo computer simulation implemented via the VEGAS code [13]. This program simulates the classical incoming and outgoing trajectories for a given scattering geometry. In the VEGAS code, the crystalline sample is described in terms of a two-dimension unit cell, which can fully retrieve layer-by-layer the crystalline structure when periodic conditions are

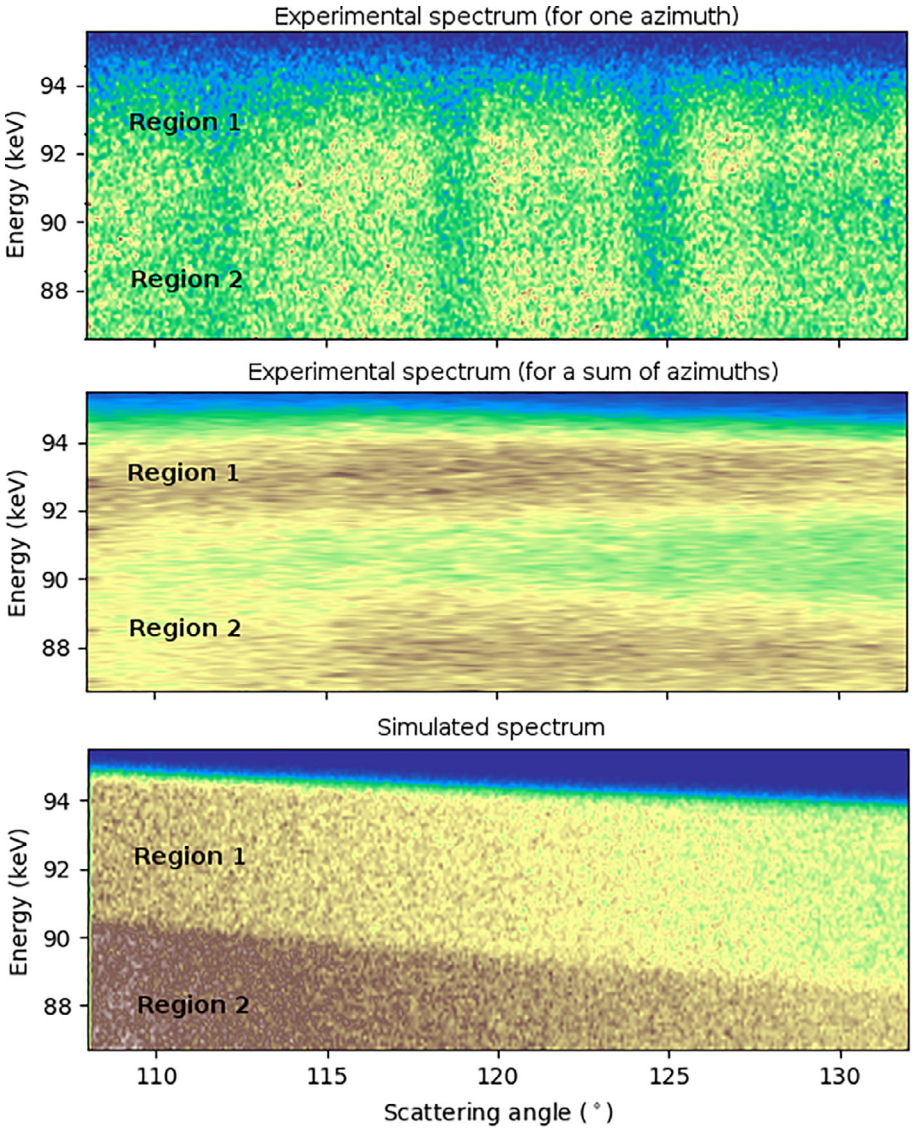

Fig. 2. 2D MEIS spectra obtained with an incoming beam of 99 keV H^+ along the ⟨1 0 0⟩ directions of the GaP crystal. For a single azimuth angle (top panel) and averaged over an azimuthal angle range of 90° (middle panel). The region 1 corresponds to the surface peak of Ga and the region 2 to the surface peak of *P* superimposed to the Ga signal. Simulation for an amorphous GaP is shown on the bottom panel for a comparison.

imposed along the surface normal. The position and nature of each atomic species within the conventional unit cell are described in a layer-by-layer grouping as shown in Fig. 3.

The VEGAS code computes two different close encounter probabilities: using only the incoming trajectories the so-called *hitting* probability (*h*) and, using the outgoing trajectories, the *detecting* probability (*d*). The last one is essentially a *hitting* probability calculated for the time-reversed outgoing trajectories starting from the detector direction. Double-alignment measurements are usually approximated by the product of *h* and *d*. The summation of the probabilities for all described sample atoms for a given scattering geometry gives the total visibility or intensity. Fig. 5 shows an example of the dependence of *d* on the polar angle for different depths; the troughs in intensity indicate blocking directions, i.e., directions on which the out-going ion trajectory is deflected by neighbouring atoms. Blocking effects are much smaller for protons backscattered from atoms at and very close to the surface.

The calculations are performed for detected ions emerging over a range of θ, ϕ angles and their *detecting* probabilities (*d*) are calculated. Channeling effects for the incoming beam can be included by considering ($h \times d$) but in what follows we neglected these effects or, equivalently, we used $h = 1$. The depth of the atoms that backscatter the protons determines the energy loss considered in the MEIS experiment. The calculated distribution of *d* values as a function of θ, ϕ can be compared with the MEIS cartography map. The comparison is usually made using a color- or gray-scale-map, and the corresponding MEIS intensity (or calculated *d* values) are represented by different colors.

The present simulations have used thermal vibration amplitudes for Ga and P atoms of 0.07 Å[14] and a scattering depth of nm, which is the depth of protons backscattered from Ga.

In order to quantify the agreement between the experimental and simulated cartographies we have used the normalized cross-correlation coefficient *r*. This coefficient is defined according as [15,16,2]:

$$r = \frac{\sum_{i,j} (f(i,j)-\overline{f})(w(i,j)-\overline{w})}{[\sum_{i,j} (f(i,j)-\overline{f})^2]^{1/2}[\sum_{i,j} (w(i,j)-\overline{w})^2]^{1/2}}. \quad (1)$$

where $f(i,j)$ and $w(i,j)$ are the intensity values obtained for a specific polar θ_i and azimuth angle ϕ_j. The $\overline{f}$ and $\overline{w}$ correspond to the mean of intensities in a experimental and simulated cartography, respectively. For a successful complete determination of the GaP crystal orientation

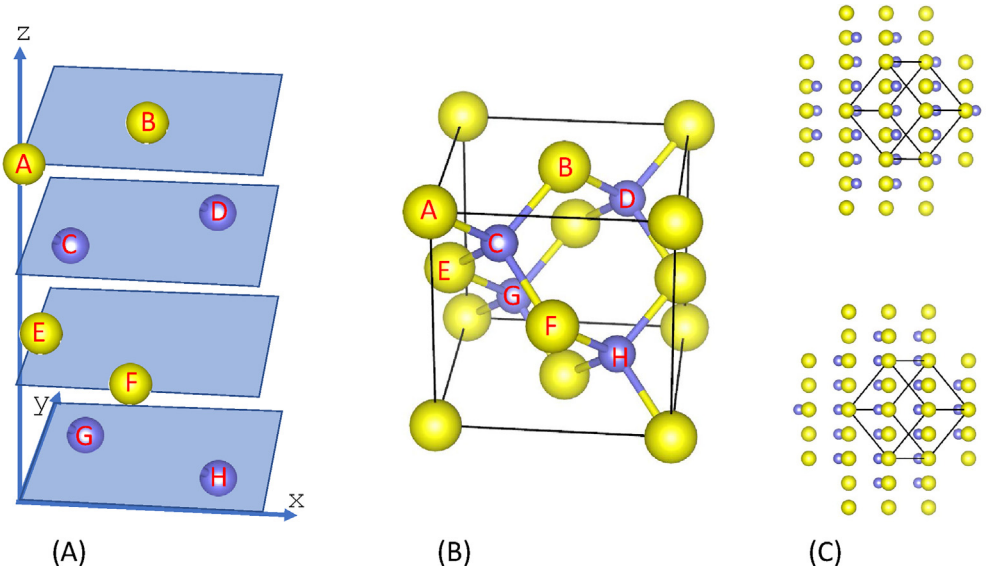

Fig. 3. Illustration on how the Vegas program models the {100} surface of a zinkblende crystal. (A) A conventional cell is divided in different layers. (B) The corresponding positions of these atoms are displayed in the conventional 3D cell. Note the absence of symmetry for rotation along the surface normal over 90°. (C) Two projections of the crystal along two [211] directions are shown. The {111} planes are vertical but the projections are not equivalent as the position of the P atoms relative to Ga is reversed.

it is required that the r value changes significantly if the experiment is compared with a theory rotated by 90° around ⟨100⟩

4. Results

In Fig. 4(A) we present the MEIS cartography for the GaP crystal. Here the scattering angle (θ_{sc}) was converted to a polar angle for the crystal unit cell (θ) according to $\theta = \pi - \theta_{sc} - \theta_{in}$, where $\theta_{in} = 25°$ is the direction of the incident beam with respect to the surface normal. Blocking effects cause reduced intensity in some directions and reveal the main crystallographic directions (the dark spots) and planes (the curved lines). Besides these blocking effects the scattering intensity can be further affected (mainly reduced) by channeling effects along the incoming path, changing the backscattering probability h. This effect is independent of the polar angle θ and is the main cause of the darker horizontal stripes superimposed on the blocking structures. Another cause of horizontal darker bands is when a crystal plane coincides with the detection plane of the TEA. In order to obtain a cartography without these channeling lines superposing the blocking structures we performed a line by line normalization. Specifically, this normalization consists of summing all intensities for a given ϕ angle, and dividing each intensity count by this sum. In addition the intensity was corrected for the dependence of the cross section on the scattering angle. The result of this procedure is shown in Fig. 4(B).

At first sight it may appear that the distribution is symmetric relative to the plane at $\phi = 90°$. However the $(1\,-1\,1)$ plane (connecting the [110] and [21$\bar{1}$] string) has extra intensity ('halo') at the inside, whereas the $(\bar{1}\,1\,1)$ plane (connecting the [211] and [101] string) has this halo on the outside. These difference of intensities are indicated by yellow and red arrows. As a consequence the measured intensity pattern is not rotational invariant for rotations over 90° along the surface normal and this makes it possible to determine the exact orientation of the GaP crystal.

Fig. 4 (C) shows the VEGAS simulations for the same angular range of the detecting probabilities summed from 2 to 6 nm. This depth range corresponds to the position of approximately the energy window of 1.5 keV used in the experiment. As the experiment the VEGAS simulation also shows the lack of fourfold symmetry. Because of this lack of

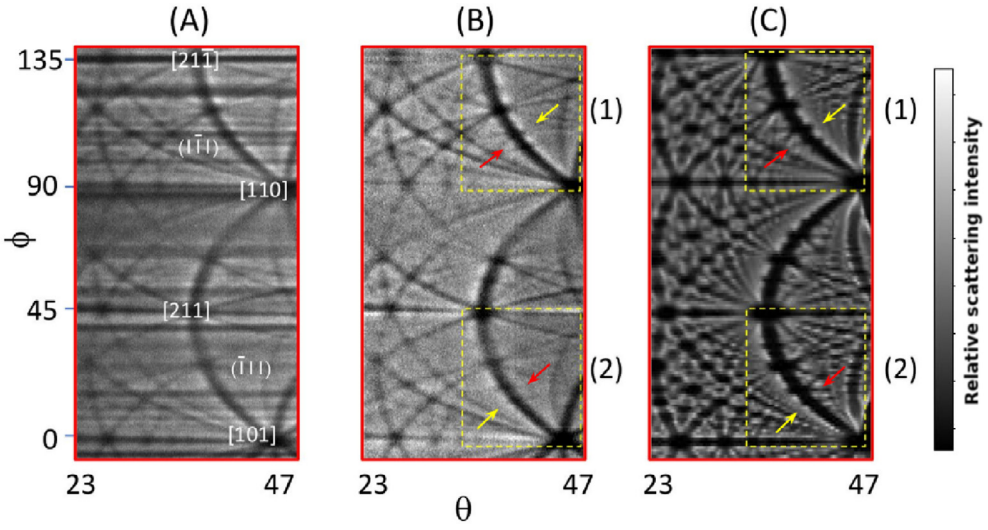

Fig. 4. (A) MEIS cartography as measured, (B) after corrections, as explained in the main text, of H^+ ions scattered from Ga atom and (C) Vegas simulation of the visibility. The angular range used for the calculation of the cross-correlation coefficients are indicated by the yellow boxes. Small scattering intensities correspond to darker shading. (For interpretation of the references to colour in this figure legend, the reader is referred to the web version of this article.)

Table 1
Cross correlation coefficients between theory and experiment for the selected angular regions (1) and (2) indicated in Fig. 4.

	Exp. B(1)	Exp. B(2)	Theory C(1)	Theory C(2)
Exp. B(1)	1.000	0.702	0.689	0.600
Exp. B(2)		1.000	0.509	0.579
Theory C(1)			1.000	0.798
Theory C(2)				1.000

symmetry, two comparisons with theory are possible, the one shown in Fig. 4, and the one with theory shifted by $\phi = 90°$. From the appearance of the halo we can decide which choice is correct, i.e. determine the full orientation of the crystal.

In order to quantify this difference we calculated the cross-correlation coefficient r according to Eq. (1) for the angular regions indicated by yellow boxes in Fig. 4(B) and (C). The resulting r values for the different possible choices of crystal orientation are reproduced in Table 1. Clearly the r values favor one choice of crystal orientation and, as expected, is equal to one comparing same regions. The variation on the r value between the experimental B(1) and B(2) occurs due to the slight difference between the rotation axis of the crystal and of the goniometer. Comparing theory regions C(1) and C(2) we get the asymmetry effect of 0.2. This value is larger than the difference observed experimentally in the r value. Therefore, misalignments reduce the value of r but the effect of the polarity remains well-resolved. In addition, the change in r value between the two choices of orientation is larger for MEIS than for EBSD [2]. It has been shown that directional effects of the incoming electron beam reveal the polarity of the crystal as well through the angular dependence of the X-ray emission yield [17]. This suggest that similar measurements would be possible by measuring the X-ray yield in a PIXE set-up while rotating the crystal through a channeling direction.

Since the MEIS technique is, in principle, depth-sensitive it is of interest to see how this asymmetry develops with depth. We display in Fig. 5 the detecting probability integrated over a unit cell. For this we choose two ϕ coordinates, 90° apart: 28° and 118°. The minimum near $\theta = 35°$ corresponds to the crossing of the {1 1 1} plane. The asymmetry develops after the first two unit cell, and persists up to the 25th unit cell layer, but with reduced amplitude. The energy window used in this experiment corresponds approximately to contributions of the 4th to 13th unit cell layer, which correspond to ≈2–6 nm.

The non-centrosymmetrical effect depends on the atom (Ga or P) where the backscattering collision takes place as can be observed in Fig. 6. In fact, the asymmetry is larger for the cartography using the P signal since neighboring Ga atoms provide a stronger blocking effect. In addition, as it can be observed in Fig. 6 the position of the halo, which

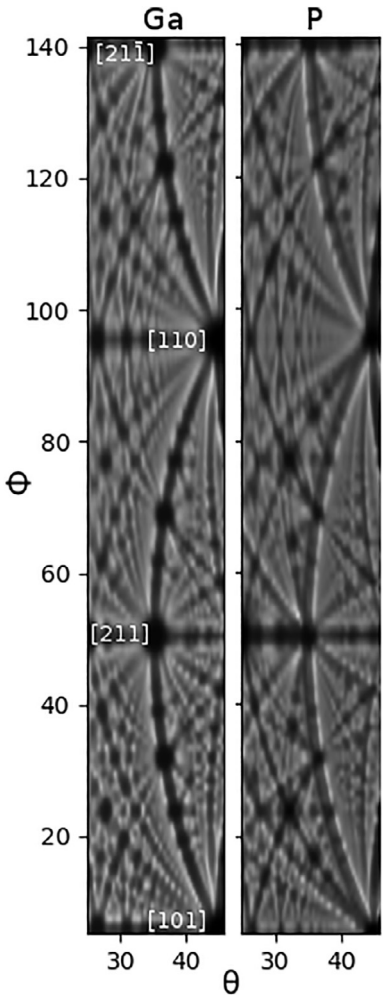

Fig. 6. Vegas simulations for the cartography obtained for scattering from Ga (left) and P (right).

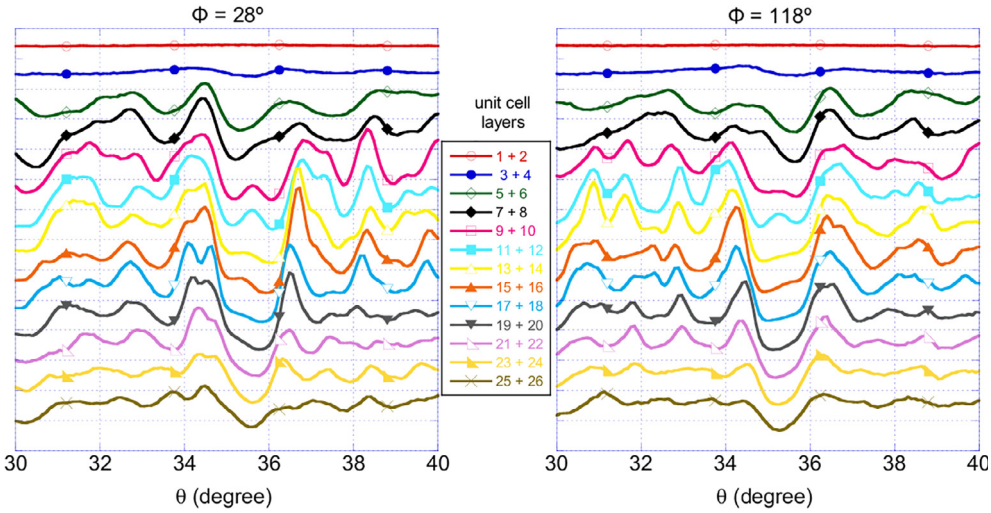

Fig. 5. Vegas simulations for the *detecting* probability d, summed over two unit cells, as a function of the polar angle for two specific azimuthal (ϕ) angles, 28° (left) and 118° (right) for 100 keV H^+ backscattered from Ga. The curves for the different unit cell layers are offset vertically for clarity. The intersection with {1 1 1} planes are at $\theta = 36°$.

presents the asymmetry, is for the P signal opposite to the one observed for the Ga signal. However, the P signal is observed in MEIS on top of the stronger Ga signal, and hence the larger P asymmetry is not easily utilized.

5. Discussion

We have shown here that ion channeling can determine the orientation of a zincblende crystal, in particular that the technique can detect that the ⟨100⟩direction has not a proper 4-fold rotational symmetry. Previous ion channeling measurements [4–6] did reveal this lack of symmetry in similar materials as well, but the intensity was measured for a single cut through a plane. The halo appearing everywhere along the {111} plane in our cartography approach makes the effect abundantly clear.

As a similar sensitivity has been demonstrated for EBSD, it is instructive to compare how the lack of 4-fold rotational axis affects both techniques. Electrons and ions are generally assumed to interact completely differently with a crystal. The former is described in terms of diffraction, with the wavelength of the electrons as the critical parameter, whereas the latter in terms of binary collisions of projectile and target atoms (although a diffraction approach has been shown to work as well, but this approach is less convenient [18,19]).

The ion channeling and EBSD experiment differ in two important aspects: the sign of the charge of the projectile and its mass (and hence wavelength). In order to make the comparison somewhat easier we did VEGAS simulations for both protons and anti-protons (with energy 100 keV) to isolate the effect of the charge and in Fig. 7 we compare these results with those for electrons (with energy 38 keV). In all cases the calculations were done for the projectile backscattering from Ga. For protons we see reduced intensity along the major planes (i.e. blocking) but for electrons and anti-protons an enhancement, clearly a consequence of the charge.

For the energy chosen the major planes (e.g. the {111} planes) have similar widths (red arrows in Fig. 7). However, the width decreases for the minor planes (as the atomic density in the planes is lower for higher-order planar directions, and hence their ability to steer the incoming beam decreases) but increases for the electron case (as the reciprocal wave vector $\boldsymbol{G}$ is larger for higher order planes). Thus the width of higher order planes is completely different, as is illustrated by the yellow arrows for a (120) plane. Also higher order diffraction effects are seen in the electron case, as is illustrated by the green arrows.

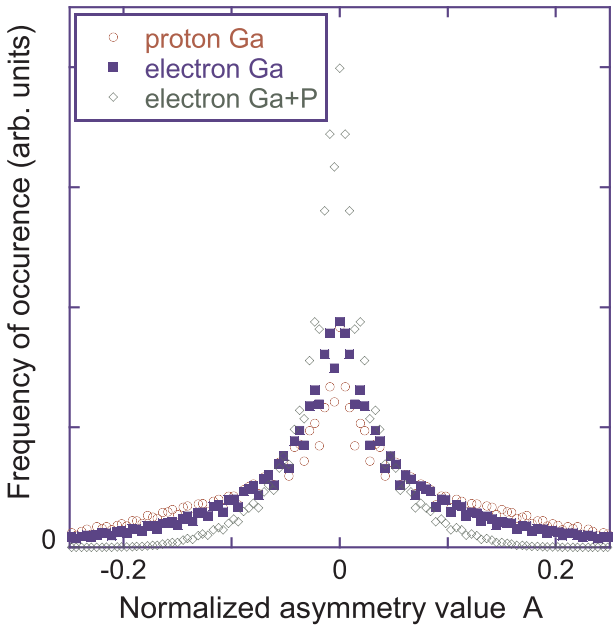

Fig. 8. A comparison of the relative asymmetry distribution in GaP for 100 keV protons scattered from Ga, 38 keV electrons scattered from Ga only or 38 keV electrons scattered from either Ga or P.

In the context of this paper the sensitivity of the probe for 90° rotation is important. This is demonstrated in the lower panel where we plot the normalized relative asymmetry of the theory $A(\theta, \phi)$ given by:

$$A(\theta, \phi) = \frac{I(\theta, \phi) - I(\theta, \phi + 90)}{I(\theta, \phi) + I(\theta, \phi + 90)}. \quad (2)$$

For both protons and electrons the strongest effect of such a rotation is near the {111} planes. The effect for rotation is more concentrated along narrow lines in the electron case, whereas for protons the enhancement is along broader lines. Considering the large differences in the underlying theory it is somewhat surprising that the electron and ion sensitivity of 90° rotation show comparable patterns. In order to get an impression of the size of the effect we plotted the distribution of the fraction of the pixels with $A(\theta, \phi)$ values in a certain range, as shown in Fig. 8. Clearly the calculated asymmetry is largest for the case of

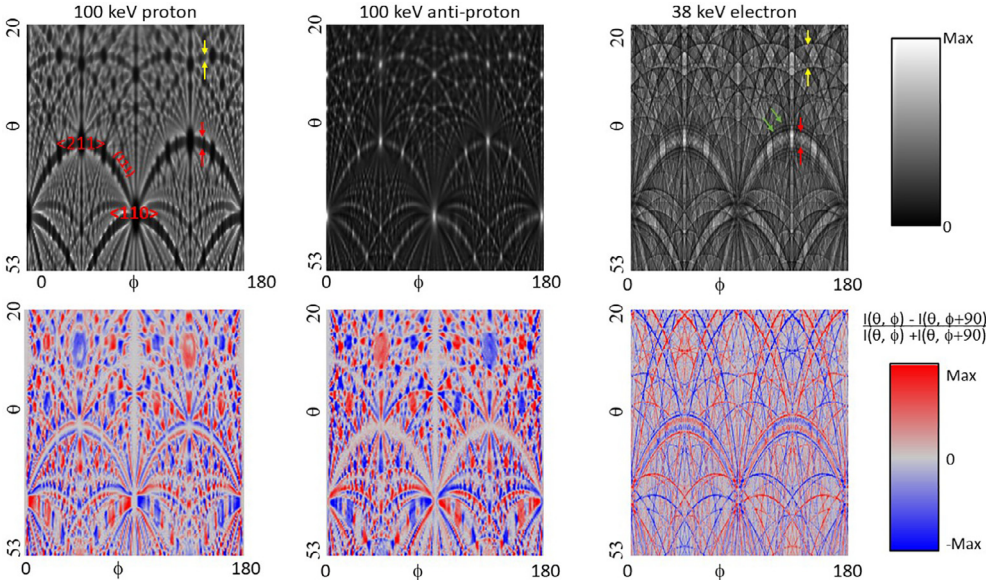

Fig. 7. A comparison of the intensities for 100 keV protons, 100 keV antiprotons and 38 keV electrons (top) and their asymmetries for rotation over 90° (bottom).

100 keV protons scattered from Ga, followed by electrons scattered from Ga. The asymmetry for the case of electrons scattered from either Ga and P (as measured in EBSD) is smallest. However the huge data acquisition rate of a phosphor screen plus camera is such that the effect can be measured with EBSD in ≈ 15 ms [20] whereas the ion scattering and ERBS measurements take several hours.

6. Conclusion

In this paper we measured the angular distribution of protons backscattered from Ga atoms in a GaP crystal. There is a clear signature, the halo along the {1 1 1} planes that changes if the crystal is rotated by 90° along the ⟨111⟩axes. It is thus possible to determine the full crystal orientation using MEIS. The asymmetries seen resemble to some degree those observed in EBSD for the same system, which is somewhat surprising as this technique is described in terms of diffraction and MEIS in terms of classical binary collisions. It is also clear, however, that data-acquisition rates are much faster in EBSD. Moreover, the smaller probe size used in the EBSD technique allows mapping the crystal surface looking for possible polarity inversion zones. Ion scattering, in its present form, is thus a poor choice to characterize multiple domains of GaP grown on Si(1 0 0), as was demonstrated to be possible by EBSD [2]. However, ion scattering is able to give the crystal information as a function of the depth, which is of interest for the characterization of strained crystalline films and nano-structures.

Acknowledgements

We are indebted to the Brazilian agencies CAPES, CNPq and FAPERGS for the partial support of this research project. MV acknowledges a travel grant of the Brazil Collaboration Scheme of the Australian National University.

References

[1] A. Beyer, J. Ohlmann, S. Liebich, H. Heim, G. Witte, W. Stolz, K. Volz, GaP heteroepitaxy on Si(001): correlation of Si-surface structure, GaP growth conditions, and Si-III/V interface structure, J. Appl. Phys. 111 (8) (2012) 083534, http://dx.doi.org/10.1063/1.4706573.

[2] G. Naresh-Kumar, A. Vilalta-Clemente, H. Jussila, A. Winkelmann, G. Nolze, S. Vespucci, S. Nagarajan, A. Wilkinson, C. Trager-Cowan, Quantitative imaging of anti-phase domains by polarity sensitive orientation mapping using electron backscatter diffraction, Sci. Rep. 7 (1) (2017) 10916, http://dx.doi.org/10.1038/s41598-017-11187-z.

[3] M. Vos, A. Winkelmann, Element-resolved kikuchi pattern measurements of non-centrosymmetric materials, Mater. Charact. 123 (2017) 328–338, http://dx.doi.org/10.1016/j.matchar.2016.11.043.

[4] A. Chami, E. Ligeon, R. Danielou, J. Fontenille, Polarity determination in compound semiconductors by channeling: application to heteroepitaxy, Appl. Phys. Lett. 52 (18) (1988) 1502–1504, http://dx.doi.org/10.1063/1.99112.

[5] L. Wielunski, M. Kwietniak, G. Pain, C. Rossouw, Polarity determination of epitaxial structures of CdTe on GaAs by channeling techniques, Nucl. Instrum. Methods Phys. Res. Sect. B 45 (1990) 459–463, http://dx.doi.org/10.1016/0168-583X(90)90875-U.

[6] D. Wijesundera, Q. Chen, K. Ma, X. Wang, B. Tilakaratne, W.-K. Chu, Planar channeling in wurtzite structured ZnO (0001): anisotropic effects due to the non-centrosymmetric structure, Nucl. Instrum. Methods Phys. Res. Sect. B 281 (2012) 77–81, http://dx.doi.org/10.1016/j.nimb.2012.03.019.

[7] R. Smeenk, R. Tromp, H. Kersten, A. Boerboom, F. Saris, Angle resolved detection of charged particles with a novel type toroidal electrostatic analyser, Nucl. Instrum. Methods Phys. Res. 195 (3) (1982) 581–586, http://dx.doi.org/10.1016/0029-554X(82)90022-2.

[8] R. Tromp, H. Kersten, E. Granneman, F. Saris, R. Koudijs, W. Kilsdonk, A new UHV system for channeling/blocking analysis of solid surfaces and interfaces, Nucl. Instrum. Methods Phys. Res. Sect. B 4 (1) (1984) 155–166, http://dx.doi.org/10.1016/0168-583X(84)90055-7.

[9] X.-F. Gu, T. Furuhara, W.-Z. Zhang, PTCLab: free and open-source software for calculating phase transformation crystallography, J. Appl. Crystallogr. 49 (3) (2016) 1099–1106, http://dx.doi.org/10.1107/S1600576716006075.

[10] M. de Albuquerque Sortica, P. Grande, G. Machado, L. Miotti, Characterization of nanoparticles through medium-energy ion scattering, J. Appl. Phys. 106 (11) (2009) 114320, http://dx.doi.org/10.1063/1.3266139.

[11] D. Jalabert, Real space structural analysis using 3D MEIS spectra from a toroidal electrostatic analyzer with 2D detector, Nucl. Instrum. Methods Phys. Res. Sect. B 270 (2012) 19–22, http://dx.doi.org/10.1016/j.nimb.2011.09.025.

[12] T. Avila, P. Fichtner, A. Hentz, P. Grande, On the use of MEIS cartography for the determination of $Si_{1-x}Ge_x$ thin-film strain, Thin Solid Films 611 (2016) 101–106, http://dx.doi.org/10.1016/j.tsf.2016.05.014.

[13] J. Frenken, R. Tromp, J. Van der Veen, Theory and simulation of high-energy ion scattering experiments for structure analysis of surfaces and interfaces, Nucl. Instrum. Methods Phys. Res. Sect. B 17 (4) (1986) 334–343, http://dx.doi.org/10.1016/0168-583X(86)90122-9.

[14] D. Gemmell, R. Holland, Blocking effects in the emergence of charged particles from single crystals, Phys. Rev. Lett. 14 (23) (1965) 945, http://dx.doi.org/10.1103/PhysRevLett. 14.945.

[15] R.C. Gonzalez, R.E. Woods, Digital Image Processing, second ed., Addison-Wesley Longman Publishing Co., Inc., Boston, MA, USA, 1992.

[16] G. Nolze, C. Grosse, A. Winkelmann, Kikuchi pattern analysis of noncentrosymmetric crystals, J. Appl. Crystallogr. 48 (2015) 1405, http://dx.doi.org/10.1107/s1600576715014016.

[17] A. Winkelmann, G. Nolze, Channeling-enhanced EDX for polarity resolved crystal orientation determination, Cryst. Res. Technol. 51 (12) (2016) 752–756, http://dx.doi.org/10.1002/crat.201600258.

[18] J.L. den Besten, L.J. Allen, D.N. Jamieson, Quantum mechanical model for rutherford backscattering of ion beams by thin crystalline lattices, Phys. Rev. B 60 (1999) 3120–3125, http://dx.doi.org/10.1103/PhysRevB.60.3120.

[19] L. Logan, M. Cottam, P. Schultz, Analytic quantum theory of planar positron channeling, Phys. Rev. B 40 (1989) 6485–6489, http://dx.doi.org/10.1103/PhysRevB.40.6485.

[20] A. Winkelmann, G. Nolze, Point-group sensitive orientation mapping of non-centrosymmetric crystals, Appl. Phys. Lett. 106 (7) (2015) 072101, http://dx.doi.org/10.1063/1.4907938.